

High permeability and bimodal resonance structure of flaky soft magnetic composite materials

Xi Liu(刘曦), Peng Wu(吴鹏), Peng Wang(王鹏), Tao Wang(王涛), Liang Qiao(乔亮), Fa-Shen Li(李发伸)

Citation: Chin. Phys. B . 2020, 29(7): 077506 . **doi:** 10.1088/1674-1056/ab8c3b
Journal homepage: http://cpb.iphy.ac.cn; http://iopscience.iop.org/cpb

What follows is a list of articles you may be interested in

Domain wall dynamics in magnetic nanotubes driven by an external magnetic field

Zai-Dong Li(李再东), Yue-Chuan Hu(胡月川), Peng-Bin He(贺鹏斌), Lin-Lin Sun(孙琳琳)

Chin. Phys. B . 2018, 27(7): 077505 . **doi:** 10.1088/1674-1056/27/7/077505

Nanoscale control of low-dimensional spin structures in manganites

Jing Wang(王静), Iftikhar Ahmed Malik, Renrong Liang(梁仁荣), Wen Huang(黄文), Renkui Zheng(郑仁奎), Jinxing Zhang(张金星)

Chin. Phys. B . 2016, 25(6): 067504 . **doi:** 10.1088/1674-1056/25/6/067504

Nonmonotonic effects of perpendicular magnetic anisotropy on current-driven vortex wall motions in magnetic nanostripes

Su Yuan-Chang, Lei Hai-Yang, Hu Jing-Guo

Chin. Phys. B . 2015, 24(9): 097506 . **doi:** 10.1088/1674-1056/24/9/097506

Temperature dependence of multi-jump magnetic switching process in epitaxial Fe/MgO (001) films

Hu Bo, He Wei, Ye Jun, Tang Jin, Zhang Yong-Sheng, Syed Sheraz Ahmad, Zhang Xiang-Qun, Cheng Zhao-Hua

Chin. Phys. B . 2015, 24(7): 077502 . **doi:** 10.1088/1674-1056/24/7/077502

Model of hybrid interfacial domain wall in ferromagnetic/antiferromagnetic bilayers

Zhang Wen, Zhai Ya, Lu Mu, You Biao, Zhai Hong-Ru, Caroline G Morgan

Chin. Phys. B . 2015, 24(4): 047502 . **doi:** 10.1088/1674-1056/24/4/047502

High permeability and bimodal resonance structure of flaky soft magnetic composite materials*

Xi Liu(刘曦)[1,†], Peng Wu(吴鹏)[1], Peng Wang(王鹏)[2], Tao Wang(王涛)[2], Liang Qiao(乔亮)[2], and Fa-Shen Li(李发伸)[2]

[1] *Key Laboratory of Opto-technology and Intelligent Control of Ministry of Education, Lanzhou Jiaotong University, Lanzhou* 730000, *China*
[2] *Institute of Applied Magnetism, Key Laboratory for Magnetism and Magnetic Materials of Ministry of Education, Lanzhou University, Lanzhou* 730000, *China*

(Received 3 January 2020; revised manuscript received 29 March 2020; accepted manuscript online 23 April 2020)

We establish a theoretical bimodal model for the complex permeability of flaky soft magnetic composite materials to explain the variability of their initial permeability. The new model is motivated by finding the two natural resonance peaks to be inconsistent with the combination of the domain wall resonance and the natural resonance. In the derivation of the model, two relationships are explored: the first one is the relationship between the number of magnetic domains and the permeability, and the second one is the relationship between the natural resonance and the domain wall resonance. This reveals that the ball milling causes the number of magnetic domains to increase and the maximum initial permeability to exist after 10 h of ball milling. An experiment is conducted to demonstrate the reliability of the proposed model. The experimental results are in good agreement with the theoretical calculations. This new model is of great significance for studying the mechanism and applications of the resonance loss for soft magnetic composite materials in high frequency fields.

Keywords: soft magnetic composite materials, bimodal resonance structure model, permeability, domain wall

PACS: 75.50.Bb **DOI:** 10.1088/1674-1056/ab8c3b

1. Introduction

Soft magnetic materials are widely used in today's society,[1–3] such as in the areas of inductors, transformers, and electrical machines. These materials are widely applied due to their complex configurations (conductive magnetic particles in an insulating matrix), large resistivity, low energy loss during magnetic circuit cycling, and excellent performance.[5,6] However, these electronic devices need to operate at higher operating frequencies with less loss to meet the requirements of both current and future applications. Therefore, improving the working frequency andreducing the loss of electronic devices have become an urgent problem to be solved.[4] To this end, we start with the resonance mechanism (a type of loss mode) to derive a solution that overcomes the Snoek limit in order to increase the permeability while increasing the operating frequency.[7]

Resonance, whether domain wall resonance or natural resonance, is a loss mode of magnetic materials, and natural resonance usually determines the operating frequency of electronic devices.[8–10] Therefore, the loss mechanism for resonance has attracted widespread attention. Usually, we use the imaginary part of the complex permeability to study this loss mechanism. It consists of two completely different mechanisms: domain wall resonance and natural resonance.[11–15] In the study by Tsutaoka, these two mechanisms were used to explain the unimodal structure.[16] Dosoudil *et al.* have extended the research of Tsutaoka by combining the two mechanisms to carry out the unimodal structure in the fitting.[17] Hank and Deng have found that there are two peaks in the imaginary part of the complex permeability. In the high frequency range, the first peak is the domain wall resonance peak, and the second one is the natural resonance peak.[18] Although the study of the two mechanisms has made significant progress, there are few reports on the relationship between the two mechanisms and how to make the domain wall resonance peak appear. This is because the domain walls themselves are insensitive, and the natural resonance peaks obscure the domain wall resonance peaks, making them difficult to identify. Only in the presence of a large number of domain walls, are the domain wall resonance peaks revealed and separated from natural resonance (as shown in Fig. 3(a)).[19]

In this paper, the ball milling method is used. This method flattens the spherical particles, greatly improves the magnetic permeability while obtaining a large number of magnetic domains, and separates the domain wall resonance peaks from the natural resonance peaks. Then, the two mechanisms are combined to establish a new model, and the relationship

*Project supported by the National Natural Science Foundation of China (Grant Nos. 11564024, 51731001, and 11574122) and the Fundamental Research Funds for the Central Universities, China (Grant No. lzujbky-2019-kb06).

†Corresponding author. E-mail: liuxi@mail.lzjtu.cn

© 2020 Chinese Physical Society and IOP Publishing Ltd

between the two mechanisms is studied and discussed. The relationship between the number of domain walls and the domain wall resonance, in addition to the relationship between the number of domain walls and the initial permeability is verified in a ball milling experiment. The experimental results are consistent with the computed results based on the model. According to the model established by the two mechanisms, the curve of the bimodal structure is also well fitted, which is a good illustration of the rationality of the model. The analysis and discussion of the relationship between the two mechanisms is presented. The proposed model provides a new way to study the high frequency loss of soft magnetic composite materials. It is also beneficial to improving the magnetic permeability and increasing the operating frequencies of soft magnetic composite materials and their related devices (inductors, transformers, and electrical machines).[20]

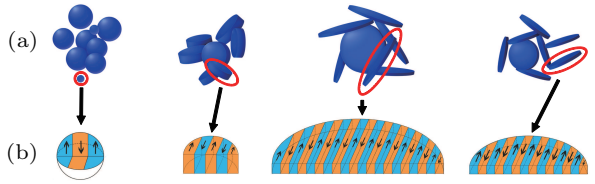


Fig. 1. Ball milling process over time, showing (a) spherical carbonyl iron particles become flaky, and thickness of flaky carbonyl iron particles gradually thin, (b) variation of magnetic domain number.

As shown in Fig. 1(a), the thickness of the flaky carbonyl iron particles is reduced from a few micrometers to a few hundred nanometers, and its diameter is still on the order of micrometers. Figure 1(b) illustrates the initial increase and subsequent decrease in the number of magnetic domains, over time. What is shown in Fig. 1(b) is not an actual variation scenario, but an example to illustrate how the number of magnetic domains changes with the thickness of the flaky carbonyl iron. The specific dimensional changes of flaky carbonyl iron are shown in Fig. 2.

2. Experimental details

Carbonyl iron particles used in the experiment are MCIP-5 carbonyl iron particles produced by Shanxi Xinghua company, and their particle size is 5 μm–6 μm. First, the powder is ground in the planetary ball mill. We use two ZrO grinding balls, respectively, with a radius of 5 mm and 3 mm. The large and small balls are mixed in the 1 : 1 mass ratio and put into a ball mill. The large ball can crush the spherical carbonyl iron particles well, and can effectively turn the spherical particles into flaky particles, and the small balls further thin the flaky particles. The ball-material ratio is 20 : 1, and the ball grinding medium is alcohol. The speed is set to be 400 r/min, and the time of ball-milling is gradually extended. The ball-milling samples were obtained with ball milling times of 4 h, 6 h, 8 h, 9 h, 10 h, 11 h, and 12 h, respectively. The scanning electron microscope (SEM) (Apreo S) is used to measure the morphology and structure of the ball-milling samples.

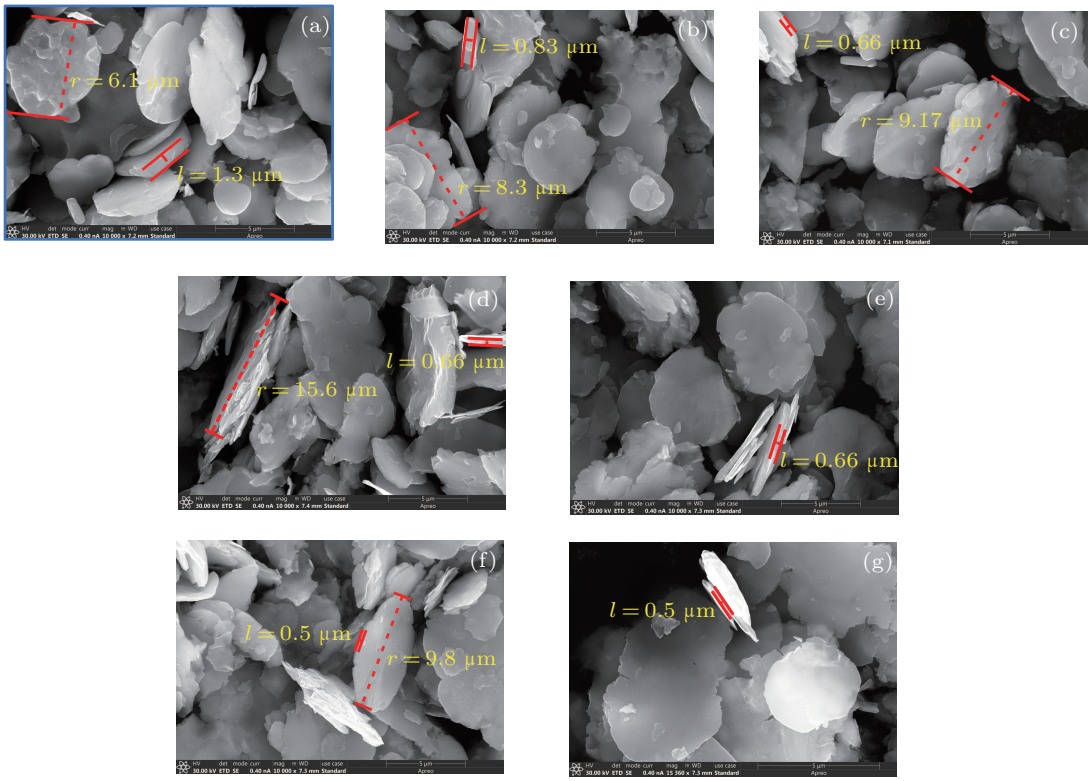


Fig. 2. Flake carbonyl iron thickness variations with ball-milling time, showing microstructures of the carbonyl iron under SEM after ball grinding for 4 h (a), 6 h (b), 8 h (c), 9 h (d), 10 h (e), 11 h (f), and 12 h (g), respectively.

We prepared a ball-milled carbonyl iron powder into a polyurethane-based composite with a volume fraction of 55%. The goal was to study the loss of the core at high frequencies, so the volume fraction was set to be as high as possible, which induced the phenomenon of falling powder. The corresponding amount of polyurethane was added to acetone and ultrasonically treated for 10 min to dissolve it; then, 0.5-g carbonyl iron particles were added into the resulting mixture. To ensure that the carbonyl iron particles and the polyurethane were fully mixed, we stirred them for 30 min ultrasonically, which also facilitated evaporating the acetone and drying the sample. The mixture was put into an annular mold which has an outer diameter of 7 mm and an inner diameter of 3.04 mm. The mixture was pressed into a ring-shaped sample with a thickness of 0.6 mm–0.8 mm at a pressure of 4 MPa. The composite permeability of the sample in a range of 0.1 GHz–18 GHz was measured by using a vector network analyzer (Agilent E8363B).

The ball milling at 400 r/min flattened the original spherical particles. As a result, the thickness of the flaky particles gradually decreased as the ball milling time increased, and the diameter gradually increased as shown in Fig. 2.

As the ball milling time is extended, the thickness of the flaky particles gradually decreases. Initially, the diameter increases and subsequently decreases. This is because the ball grinding time is excessive, during which the original larger flake particles are broken into smaller flake particles. This lead the diameter-thickness ratio to first increase and then decrease. This change in the ratio affects the permeability: the permeability also initially increases and then decreases (as shown in Fig. 3(b)), which is in accordance with Walser's theory.[21]

This variation in the diameter-thickness ratio also affects the change in the number of magnetic domains. This number is related to the decreasing in thickness of the flaky particles over time. The width D of the magnetic domains is proportional to the thickness l of the sample particles. In our study, the thickness reduction caused by ball milling is far from the critical value reached when a single domain structure forms. For a spherical ferromagnetic particle, the critical radius of single domain for carbonyl iron is 2 nm; for a flaky particle with a thickness of 600 nm, the critical width of single domain for carbonyl iron is approximately 45 nm, both values are much smaller than the size of our balling milling particles.[22]

As the thickness l decreases, the number of magnetic domains per unit volume increases.[23] In the early stage of the ball milling process, the number of magnetic domains increases as the thickness decreases. Over time, the number of domain walls increases with the number of magnetic domains increasing. When large flaky particles break from prolonged and excessive ball milling, the thickness of the flaky particles continues to thin, but its diameter can also be significantly reduced. As a result, there is an increase in the number of magnetic domains per unit volume. However, the total volume decreases as the diameter decreases, and the number of magnetic domains begins to decrease as shown in Fig. 1. As a result, the number of magnetic domains increases and then decreases over ball milling time. This process also causes the number of domain walls to increase and then decrease. The number of domain walls affects the variation of the domain wall resonance peaks. According to the experimental results, we find that the trend of domain wall resonance peaks is consistent with the trend of the number of magnetic domains and the number of domain walls. So the results are also consistent with the variation of the initial permeability.[19]

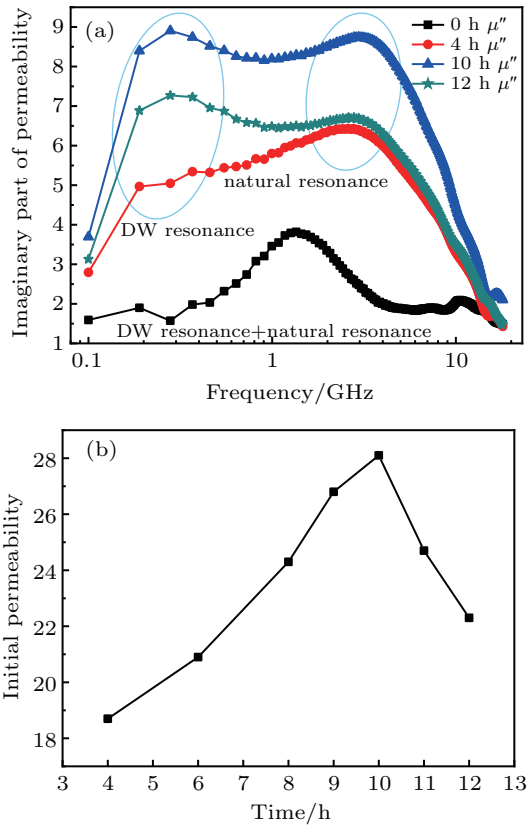


Fig. 3. (a) Separation of domain wall resonance and natural resonance in imaginary part of magnetic permeability for different ball milling times (For improving readability, only four representative times are illustrated); (b) initial permeability varying with time.

In summary, the ball milling process causes the aspect ratio of the flaky particles to change. This changes the number of magnetic domains and domain walls, thereby affecting the variation of the domain wall resonance peaks and the magnetic permeability.

3. Modeling

The model is established by combining the two mechanisms of domain wall resonance and natural resonance. On

the one hand, the permeability affected by the natural resonance mechanism is partly calculated according to the LLG equation, and we consider the spatial random distribution of the easy magnetization axis. Since the sample is made from a carbonyl iron compound embedded in polyurethane, we calculate the effective permeability through the effective medium theory.[24] On the other hand, the permeability affected by the domain wall resonance is calculated according to the domain wall motion equation. The complex permeability of the sample is obtained by combining the two. Although we do not take into consideration the influence of the skin effect in the proposed model, the theoretical calculation results and experimental results have confirmed the model's reliability.

3.1. Natural resonance

In the absence of an external magnetic field, the distribution of magnetization intensity is always in the direction of the lowest energy due to the magnetic anisotropic energy. Therefore, we can use the equivalent anisotropic field H_k to replace the influence of magnetic anisotropic energy. We can use the LLG equation to calculate the effective permeability

$$\frac{\mathrm{d}M}{\mathrm{d}t} = \gamma(M \times \boldsymbol{H}_k) + \frac{\alpha}{M}\boldsymbol{M} \times \frac{\mathrm{d}\boldsymbol{M}}{\mathrm{d}t}, \tag{1}$$

where γ is the gyromagnetic rotation ratio and α is the damping coefficient.[25,26]

Since the magnetic field lags behind the external magnetic field in the alternating electromagnetic field and thus produces a phase difference, we can use the permeability in the complex form as follows:

$$\begin{aligned} \boldsymbol{H} &= \boldsymbol{H}_k + \boldsymbol{h}\mathrm{e}^{\mathrm{j}\omega t - \phi \boldsymbol{kr}}, \\ \boldsymbol{M} &= \boldsymbol{M}_\mathrm{s} + \boldsymbol{m}\mathrm{e}^{\mathrm{j}\omega t - \phi \boldsymbol{kr}}, \end{aligned} \tag{2}$$

where M_s is the saturation magnetization intensity, and h and m are the small fluctuation coefficients. Using Maxwell's equation and substituting Eq. (1) into Eq. (2), the following permeability tensor can be obtained:

$$\mu = \frac{1}{\varepsilon}\left(\frac{\delta}{\mathrm{j}w}\right)^2 \begin{bmatrix} 1-\sin^2\theta\cos^2\phi & -\sin^2\theta\sin\phi\cos\phi & -\sin\theta\cos\theta\cos\phi \\ -\sin^2\theta\sin\phi\cos\phi & 1-\sin^2\theta\sin^2\phi & -\sin\theta\cos\theta\sin\phi \\ -\sin\theta\cos\theta\cos\phi & -\sin\theta\cos\theta\sin\phi & 1-\cos^2\theta \end{bmatrix}, \tag{3}$$

where δ is obtained from

$$\delta = \mathrm{j}\omega(\mu_0\varepsilon)^{1/2}\left\{\frac{\left(\mu^2-\mu-\kappa^2\right)\sin^2\theta + 2\mu - \left[\left(\mu^2-\mu-\kappa^2\right)^2\sin^4\theta + 4\kappa^2\cos^2\theta\right]^{1/2}}{2\left[(\mu-1)\sin^2\theta+1\right]}\right\}, \tag{4}$$

μ and κ being complex numbers in the δ as shown below:

$$\begin{aligned} \mu &= 1 + \frac{\omega_0'\omega_m}{\omega_0'^2-\omega^2} \\ &= 1 + \frac{\omega_0\omega_m\left[\omega_0^2-\omega^2\left(1-\alpha^2\right)\right]}{\left[\omega_0^2-\omega^2\left(1+\alpha^2\right)\right]^2+4\omega^2\omega_0^2\alpha^2} \\ &\quad -\mathrm{j}\frac{\omega\alpha\omega_m\left[\omega_0^2+\omega^2(1+\alpha^2)\right]}{\left[\omega_0^2-\omega^2(1+\alpha^2)\right]^2+4\omega^2\omega_0^2\alpha^2}, \\ \kappa &= -\frac{\omega\omega_m}{\omega_0'^2-\omega^2} \\ &= -\frac{\omega\omega_m\left[\omega_0^2-\omega^2\left(1+\alpha^2\right)\right]}{\left[\omega_0^2-\omega^2\left(1+\alpha^2\right)\right]^2+4\omega^2\omega_0^2\alpha^2} \\ &\quad +\mathrm{j}\frac{2\omega^2\alpha\omega_m\omega_0}{\left[\omega_0^2-\omega^2\left(1+\alpha^2\right)\right]^2+4\omega^2\omega_0^2\alpha^2}, \end{aligned} \tag{5, 6}$$

with $\omega_m = \gamma M_0\omega_0 = \gamma H_k\omega_0' = \omega_0 + \mathrm{j}\omega\alpha$ (ω being the circular frequency, $\omega = 2\pi f$, 0.1 GHz$\leqslant f \leqslant$ 18 GHz and M_0 being the saturation magnetization at 0 K).

In this process, we introduce the permeability tensor. We take the spatial orientation of the magnetic moment into consideration. This makes the damping factor α less than one, which is more in line with the physical meaning. If we use the LLG equation directly in the model, the damping factor α may be greater than one.

Since the distribution directions of the easy magnetic axes are random, we choose 10^4 single domains, and each domain can produce the intrinsic permeability at random angles (θ and ϕ)[27] as follows:

$$\langle\mu_\mathrm{i}\rangle = \frac{\sum_1^N \mu_\mathrm{i}(\theta,\phi)}{N}. \tag{7}$$

The intrinsic permeability μ_i can be calculated through the permeability tensor as follows:

$$\mu_\mathrm{i} = \mathrm{Eigenvalue}(\langle\mu_\mathrm{i}\rangle). \tag{8}$$

From Eq. (8) we can obtain the theoretical intrinsic permeability μ_i.

3.2. Domain wall resonance

We can obtain the domain wall motion equation which is based on the properties of the domain wall that Doring

proposed.[28] Using Eq. (9) as the 180° domain wall's equation (here we only consider the 180° domain wall, if we consider the 90° domain wall, the term on the right-hand side of the equation becomes $\sqrt{2}M_sH$):

$$m_w\frac{d^2z}{dt^2}+\beta\frac{dz}{dt}+\alpha^*z=2M_sH. \tag{9}$$

For a variable magnetic field with a small amplitude, $\tilde{H}=H_m e^{i\omega t}$, the displacement distance z of domain wall can be expressed as $\tilde{z}=z_m e^{i\omega t}$. Therefore, substituting it into Eq. (9) we obtain

$$z_m\left(-\omega^2m_w+i\omega\beta+\alpha^*\right)=2M_sH_m. \tag{10}$$

The z_m is expressed as

$$z_m=\frac{2M_sH_m}{\alpha^*\left(1-\frac{m_w}{\alpha^*}\omega^2+i\omega\frac{\beta}{\alpha^*}\right)}, \tag{11}$$

where m_w is the effective mass of the domain wall per unit area, β the damping coefficient of the domain wall, and α^* the elastic recovery coefficient. According to the theory of static magnetics, after the 180° domain wall moves a distance z, the increase of magnetization in the magnetic field direction is $2M_sz$. As a result, the change of the magnetization in unit volume is ΔM is as follows:

$$\Delta M=\frac{2M_sz}{D}. \tag{12}$$

The complex magnetic susceptibility $\tilde{\chi}$ is expressed as

$$\begin{aligned}\tilde{\chi}&=\frac{\Delta\tilde{M}}{\tilde{H}}=\frac{4M_s^2}{\alpha^*D}\cdot\frac{1}{\left[1-(\omega/\omega_r)^2\right]+i\omega/\omega_\tau}\\&=\chi_0\frac{1}{\left[1-(\omega/\omega_r)^2\right]+i\omega/\omega_\tau},\end{aligned} \tag{13}$$

where χ_0, ω_r, and ω_τ are defined as follows:

$$\chi_0=4M_s^2/\alpha^*D, \tag{14}$$

$$\omega_r=\sqrt{\alpha^*/m_w}, \tag{15}$$

$$\omega_\tau=\alpha^*/\beta, \tag{16}$$

with χ_0 being the static magnetic susceptibility when the external magnetic field and magnetizing frequency are both approach to zero, ω_r the circular frequency of eigenvibration of the domain wall, and ω_τ the circular frequency of the relaxation frequency. In the absence of an external magnetic field, the static magnetic susceptibility is defined as[29]

$$\chi_a=\frac{4M_s^2\cos^2\theta}{\alpha^*}S. \tag{17}$$

Because adopted in this experiment is magnetic powder for the carbonyl iron powder, its easy magnetization axis is $\langle100\rangle$, 180° domain wall parallel to the edge. Here, $\cos^2\theta=1$; when only considering the domain wall area per unit volume when $S=1/D$, equation (17) is the same as Eq. (14).[30]

We obtain the permeability of the domain wall μ_w from the following equation:

$$\mu_w=\chi_0\frac{1}{\left[1-(\omega/\omega_r)^2\right]+i\omega/\omega_\tau}. \tag{18}$$

At this point, we can combine the natural resonance (Eq. (8)) and the domain wall resonance (Eq. (18)) to obtain the final permeability

$$\mu'=\mu_i+\mu_w+1. \tag{19}$$

3.3. Effective medium theory

The flake magnetic powder particles are dispersed in the insulating matrix. In the composite system, in order to obtain its effective permeability, Bruggeman's effective medium theory can be used as follows (a correction parameter included):[31]

$$\mu_{eff}=1+\frac{p\left(\mu_{app}-1\right)}{1+N\left(\mu_{app}-1\right)\left(1-p/p_c\right)}, \tag{20}$$

$$\mu_{app}=A\times\mu', \tag{21}$$

where A is the correction parameter, N the demagnetization factor, and p_c the penetration threshold.[31]

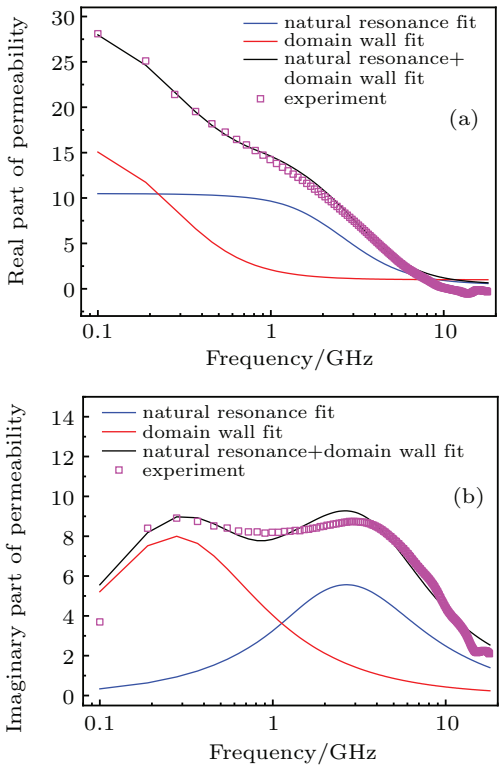


Fig. 4. Comparison between the magnetic permeability of the proposed model and the experimental results, illustrating an example by using flaky carbonyl iron with a speed of 400 min/h and ball milling for 10 h for (a) real part of magnetic permeability, and (b) imaginary part of magnetic permeability.

The two mechanisms have different contributions in the imaginary part of the magnetic permeability. The contribution of the domain wall resonance is mainly in the MHz band, and the natural resonance mainly contributes to the GHz band (as shown in Fig. 4).

The sample milled by balls for 10 h is taken for example. Under the joint action of the two mechanisms, the experimental results are basically consistent with the theoretical results, which proves the reliability of our model.

4. Results and discussion

4.1. Relationship between two resonance mechanisms

According to the fitting process and the results, it is found that the natural resonance and the domain wall resonance are controlled by two different mechanisms. In addition, there are five parameters in the fitting process: the equivalent anisotropic field H_k, the damping factor α, the static magnetic susceptibility χ_0, the circular frequency of eigenvibration of the domain wall ω_r, and the circular frequency of relaxation frequency ω_τ, which are illustrated in Fig. 5.

The model is mainly divided into two parts: the domain wall resonance and the natural resonance. In the domain wall resonance part, χ_0, ω_r, and ω_τ are the main parameters, whereas H_k and α are the main parameters in the natural resonance part. This indicates that the five parameters are not independent of each other, and their relationships are explored below.

According to the fitting results, both H_k and χ_0 are the main factors affecting the imaginary part of the magnetic permeability, H_k and χ_0 have completely opposite trends, and both H_k and χ_0 are affected by a common factor, the magnetocrystalline anisotropy constant K. The equivalent anisotropic field H_k and the magnetocrystalline anisotropy constant K have the same variation trend. From the fitting results, we find that H_k first decreases and subsequently increases (as shown in Fig. 5(a)), so K also initially decreases and then increases.

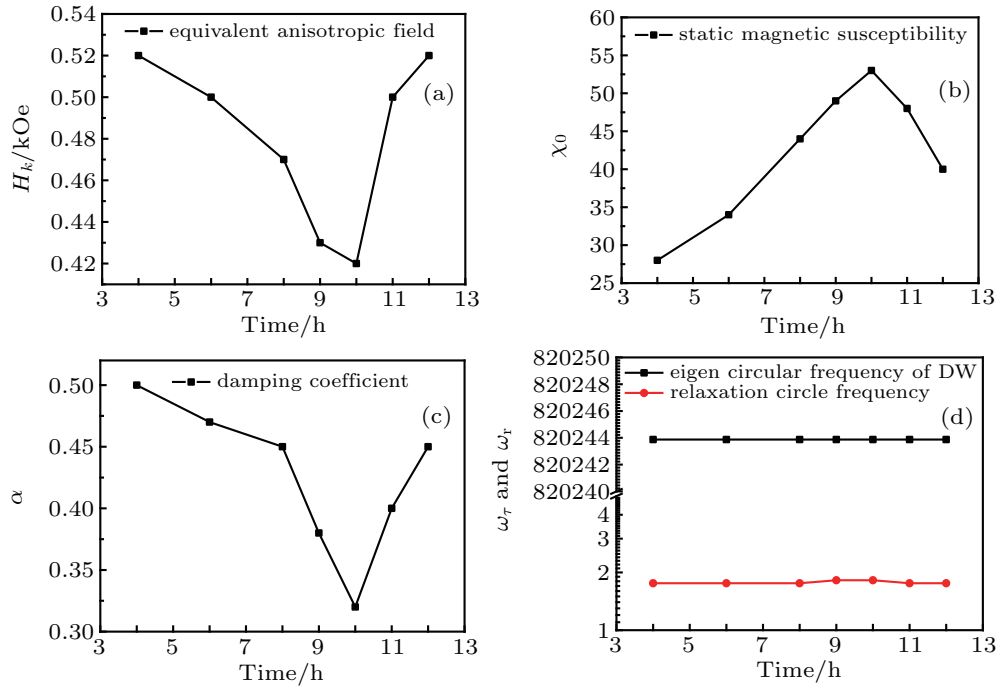


Fig. 5. Fitting results of five parameters under different ball grinding times, showing (a) equivalent anisotropic field H_k varying with ball grinding time, (b) static magnetic susceptibility χ_0 varying with ball grinding time, (c) damping factor α varying with ball grinding time, (d) circular frequency of eigenvibration of domain wall ω_r and the circular frequency of relaxation frequency ω_τ varying with ball grinding time. The unit 1 Oe = 79.5775 A·m^{-1}.

The fitting result of the static magnetic susceptibility χ_0 is completely opposite to the equivalent anisotropic field H_k, which is also caused by the magnetocrystalline anisotropy constant K. We can learn from Eq. (14) that χ_0 is controlled by α^* and D together, and α^* can be expressed as

$$\alpha^* = \frac{2\pi\sigma_w}{a'}, \tag{22}$$

where $\sigma_w = 2\pi\sqrt{JS^2K/a'}$ is the wall energy per unit area (J is the exchange integral).[32]

By Eq. (14), in the ball mill when the milling time is less than 10 h, χ_0 increases as α^*D decreases, χ_0 reaches its maximum at a milling time of 10 h, and then after the ball mill operates for more than 10 h, χ_0 decreases with the increase of α^*D (as shown in Fig. 5(b)). Equation (22) shows that α^* is affected by the magnetocrystalline anisotropy constant K: it increases with K increasing. With the extension of the ball

grinding time, D decreases with the gradual decrease of the thickness of flake particles (throughout the ball milling process, the thickness of the flakes is reduced as the ball milling time increases[21]). So, during the ball milling time before 10 h, χ_0 increases with the decrease of α^* and D. After 10 h of milling time, α^* and D enter into a competitive relationship. The D decreases as the ball milling continues to increase; therefore, when D continuously decreases, χ_0 only shows a decreasing trend when α^* is in an increased state and dominates. According to the variation of α^*, we can see that the variation of the magnetocrystalline anisotropy constant K also first decreases and then increases. This result is consistent with the variation in K obtained from the fitting result of H_k.

The H_k and χ_0 are the two main controlling parameters of the natural resonance and the domain wall resonance, respectively. They are both affected by K. As K initially decreases and then increases, the parameters respond as follows: H_k first decreases and then increases; χ_0 first increases and then decreases (K affects χ_0 through influencing α^*).

The damping factor α ($\alpha = 4\pi\mu_0\lambda/\gamma M_s$) varies proportionally with the relaxation frequency λ. According to Fig. 5(c), the damping factor α first decreases and then increases with time increasing; as α is directly proportional to λ, λ should also first decrease and then increase with time increasing. When the ball milling time reaches 10 h, the relaxation frequency λ reaches a minimum value.

We bring the damping factor of the domain wall β ($\beta = 2\pi\mu_0\lambda\sigma_w/\gamma^2 A$) into Eq. (16), and transform ω_τ into

$$\omega_\tau = \frac{\gamma^2 A}{a'\mu_0\lambda}, \tag{23}$$

where λ is the relaxation frequency. Through the fitting process, it is found that ω_τ can control the position of the domain wall resonance peak. It is known from Eq. (23) that ω_τ is influenced by λ and a'. Here, we have identified a' as a constant (explained below), so λ becomes its main influencing factor.

The circular frequency of eigenvibration of the domain wall ω_r is determined jointly by m_w and α^*, which are expressed as

$$m_w = \frac{\mu_0\sigma_w}{2\gamma^2 A}, \tag{24}$$

$$\alpha^* = \frac{2\pi\sigma_w}{a'}, \tag{25}$$

where σ_w is the wall energy per unit area, and A is the exchange stiffness constant.[27]

Substituting Eqs. (24) and (25) into Eq. (15) results in

$$\omega_r = \sqrt{\frac{4\pi\gamma^2 A}{\mu_0 a'}}. \tag{26}$$

It is known from Eq. (26) that only the lattice constant a' can affect the variation of ω_r. As a ball milling leads to the deformation of particles, it is affected by its lattice constant a'. However, according to the fitting result, ω_r is a constant as shown in Fig. 5(d). This shows that the variation of a' does not substantially affect ω_r. In order to facilitate understanding and calculation, we assume a' and ω_r to be constant.

From the fitting results we obtain that the circular frequency of eigenvibration of the domain wall ω_r is much larger than the circular frequency of the relaxation frequency ω_τ as shown in Fig. 5(d). This indicates that the resonance type is a relaxed domain wall resonance, which is in full agreement with the experimental result. This also illustrates the rationality of our fit.

The five parameters involved in the fit are not independent of each other. Among them, H_k and χ_0 are controlled by K, α and ω_τ are controlled by λ, and ω_r is basically constant. The domain wall resonance and the natural resonance are related by K and λ, thereby linking the two mechanisms together. By fitting the results, the experimental data and the fitting results are basically coincident as shown in Fig. 6, which further proves the feasibility of our model and the rationality of the results.

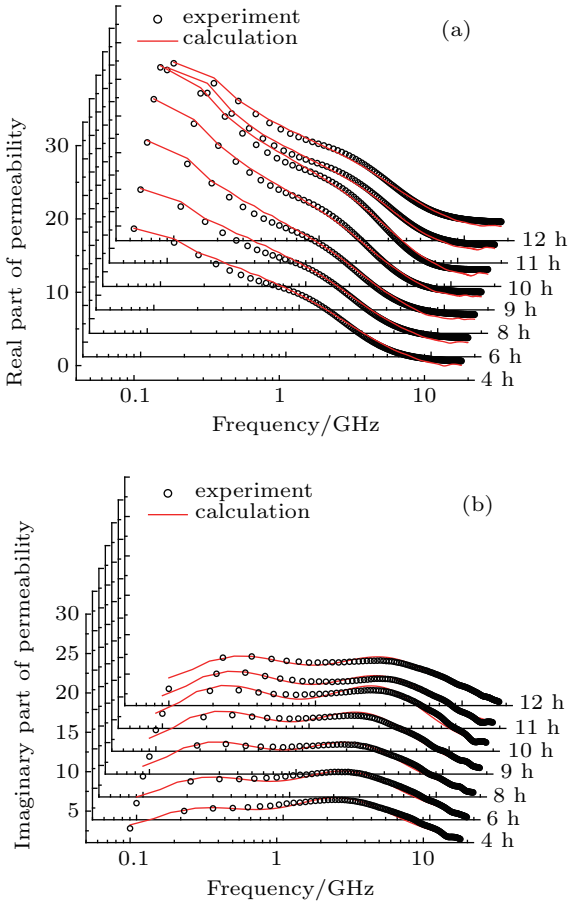


Fig. 6. Comparisons between model calculations and experimental results for real and imaginary parts of the magnetic permeability at different frequencies and ball milling times.

4.2. Relationship between domain wall and magnetic permeability

From the magnetic spectrum, we find obvious changes in the domain wall resonance peaks. This is due to the increase in the number of domain walls,[19] which causes the domain wall resonance peaks to separate from the natural resonance peaks. As the number of domain walls first increases and then decreases, the intensity of the domain wall resonance peaks correspondingly changes (*i.e.*, first increases and decreases). This is the same as the change in the initial permeability. In the domain wall resonance mechanism, χ_0 is the main factor controlling the intensity of the domain wall resonance peak, and its change trend is the same as those of the peak strength and initial permeability of the domain wall resonance peak. The variation in the number of magnetic domains and domain walls lead to a certain change in χ_0. In Eq. (15), χ_0 is proportional to μ_w. Therefore, in the process of changing the number of magnetic domains and domain walls, the initial magnetic permeability is affected, resulting in the same trend as shown in Fig. 7.

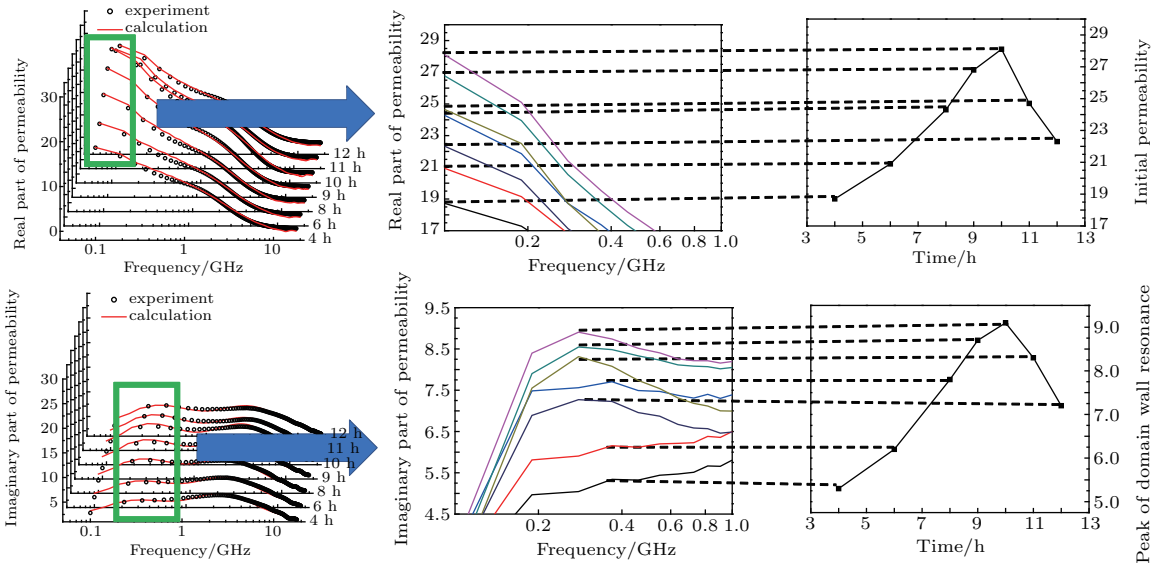


Fig. 7. Comparisons between initial permeability (0.1 GHz–1.0 GHz) and domain wall resonance peak intensities of the polyurethane-based flaky carbonyl iron composites with a 55%-volume fraction of flaky carbonyl iron, showing variation of domain wall resonance peak intensity to be consistent with variation of initial permeability.

In the ball milling process, the increase in the number of magnetic domains and domain walls caused by the flattening not only cause the separation of the domain wall resonance peaks and the natural resonance peaks, but also contribute to an increase in the magnetic permeability. The enhancement of the domain wall resonance peak and the increase of the initial magnetic permeability clearly embody this result. Furthermore, the initial decrease then subsequent increase of H_k, as well as the initial increase then decrease of χ_0 in the fitting parameters also verify this result and confirm the reliability of the model.

5. Conclusions

In our experimental study, we improved the permeability of carbonyl iron in ball milling by changing the particle morphology and improving the width-and-thickness ratio of the sample. The preparation of flaky carbonyl iron can be completed by ball milling alone. Therefore, the efficiency is very high, but for different ball mills there need different ball-to-material ratios and size-to-ball ratios. In the process of ball grinding, the deepening of the flattening process not only increases not only the magnetic permeability, but also the magnetic domains and domain walls. The increase in the number of magnetic domains and domain walls both further contribute to magnetic permeability. However, when excessive ball grinding occurs, the originally large and thin flake particles are broken into small and thin fragments, the diameter-thickness ratio decreases, the magnetic permeability decreases, and the number of magnetic domains and domain walls both also decrease. Therefore, the identification of the optimal ball milling time is essential.

We also established a new model with a bimodal structure (two mechanisms). In the model we consider the spatial random distribution, and then we obtain the permeability $\mu' = \mu_i + \mu_w + 1$. We also consider the influence of effective medium theory, and constrain the damping coefficient values to be less than one. If the damping coefficient exceeds one, the magnetic moment is ahead of the microwave field, which is not consistent with physical scenarios. Only when the damping coefficient is less than one, does the magnetic moment lag behind the microwave field and the precessional motion.

By relating the variation of the domain width with the

variation of the domain number in the unit volume, several factors affecting the domain wall resonance are discussed. It is found that the domain wall resonance is related to not only the number of domain walls, but also the magnetocrystalline anisotropy constant K and the relaxation frequency λ. Among the five fitting parameters, H_k and χ_0 are affected by K, whereas α and ω_τ are affected by λ. In this way, both the domain wall resonance and the natural resonance are jointly controlled by K and λ. Thus we can relate the domain wall resonance to the natural resonance by studying K and λ.

References

[1] Brosseau C and Talbot P 2005 *J. Appl. Phys.* **97** 104325
[2] Viau G, Ravel F, Acher O, Fiévet-Vincent F and Fiévet F 1995 *J. Magn. Magn. Mater.* **377** 140
[3] Ding J, Shi J, Chen L F, Deng C R, Fu S H and Li Y 2002 *J. Magn. Magn. Mater.* **247** 249
[4] Silveyra J M, Ferrara E, Huber D L and Monson T C 2018 *Science* **362** 1
[5] Shokrollahi H and Janghorban K 2007 *J. Mater. Process. Technol.* **189** 1
[6] Taghvaei A H, Shokrollahi H, Janghorban K 2009 *J. Alloys Compd.* **481** 681
[7] Snoek J 1948 *J. Phys.* **14** 207
[8] Zhang X F, Dong X L, Huang H, *et al.* 2006 *Appl. Phys. Lett.* **89** 053115
[9] Wu M Z, Zhang Y D, Hui S, *et al.* 2002 *Appl. Phys. Lett.* **80** 4404
[10] Liao S B 2000 *Physics of Ferromagnetism* (Beijing: Science Press) pp. 1–50
[11] Rado G T, Wright R W and Emerson W H 1950 *Phys. Rev.* **80** 273
[12] Polder D and Amit J 1953 *Rev. Mod. Phys.* **25** 89
[13] Guyot M and Cagan V 1982 *J. Magn. Magn. Mater.* **27** 202
[14] Guyot M, Merceron T, Cagan V and Messekher A 1988 *Phys. Status Solidi* **106** 595
[15] Jankovskis J, Yurshevich V and Rankis G 1997 *J. Phys. Colloq.* C1-203
[16] Tsutaoka T 2003 *J. Appl. Phys.* **93** 5
[17] Dosoudil R, Usakova M, Slama J and Gruskova A 2008 *J. Acta Phys. Pol. A* **113** 1
[18] Han M, Deng L 2007 *Appl. Phys. Lett.* **90** 011108
[19] Saitoh E, Miyajima H, Yamaoka T and Tatara G 2004 *Nature* **432** 7014
[20] Silveyra J M, Ferrara E, Huber D L and Monson T C 2018 *Science* **362** 6413
[21] Walser R M, Win W, Valanju P 1998 *J. IEEE Trans. Magn.* **34** 1390
[22] Chikazumi S 1997 *Physics of Ferromagnetism* (New York: Soshin Chikazumi) pp. 441–455
[23] Chikazumi S 1997 *Physics of Ferromagnetism* (New York: Soshin Chikazumi) pp. 453–456
[24] Qiao L, Wen F, Wei J, Wang J and Li F 2008 *J. App Phys.* **103** 063903
[25] Wu L Z, Ding J, Jiang H B, *et al.* 2008 *J. Appl. Phys.* **99** 65
[26] Soohoo R F 1985 *Microwave Magnetics* (New York: Harper & Row) pp. 182–184
[27] Wu L Z, Ding J, Jiang H B, *et al.* 2006 *J. Appl. Phys.* **99** 083905
[28] Wu Y, Han M, Tang Z, Deng and L 2014 *J. Appl. Phys.* **115** 163902
[29] Doring W 1948 *Z. Naturforsch* **3a** 373
[30] Chikazumi S 1997 *Physics of Ferromagnetism* (New York: Soshin Chikazumi) pp. 480–491
[31] Becker R and Doring W 1939 *Ferromagnetismus* (Berlin: Springer) p. 153
[32] Chikazumi S 1997 *Physics of Ferromagnetism* (New York: Soshin Chikazumi) pp. 411–417